frontiers | Frontiers in Materials

TYPE Original Research
PUBLISHED 06 January 2023
DOI 10.3389/fmats.2022.1118952

OPEN ACCESS

EDITED BY
Atefeh Karimzadeharani,
Leibniz Institute for Solid State and Materials Research Dresden (IFW Dresden), Germany

REVIEWED BY
Yong A. Zhang,
University of Science and Technology Beijing, China
Rahmiye Zerrin Yarbay,
Bilecik Şeyh Edebali University, Türkiye

*CORRESPONDENCE
Wei Wang,
wangwei2@imech.ac.cn

†These authors have contributed equally to this work and share first authorship

SPECIALTY SECTION
This article was submitted to Computational Materials Science, a section of the journal Frontiers in Materials

RECEIVED 08 December 2022
ACCEPTED 28 December 2022
PUBLISHED 06 January 2023

CITATION
Tao Y, Cheng W and Wang W (2023), Atomistic tensile deformation mechanisms in a CrCoNi medium-entropy alloy with gradient nano-grained structure at cryogenic temperature.
Front. Mater. 9:1118952.
doi: 10.3389/fmats.2022.1118952

Atomistic tensile deformation mechanisms in a CrCoNi medium-entropy alloy with gradient nano-grained structure at cryogenic temperature

Yuhao Tao[1†], Wenqiang Cheng[2,3†] and Wei Wang[2*]

[1]Department of Mechanical Engineering, RWTH Aachen University, Aachen, Germany, [2]State Key Laboratory of Nonlinear Mechanics, Institute of Mechanics, Chinese Academy of Sciences, Beijing, China, [3]School of Engineering Sciences, University of Chinese Academy of Sciences, Beijing, China

Large-scale molecular dynamics (MD) simulations have been utilized to reveal the atomistic deformation mechanisms of a CrCoNi medium-entropy alloy (MEA) with gradient nano-grained (GNG) structure in the present study. Strong strain hardening was observed in the gradient nano-grained structure at the elasto-plastic transition stage, which could be attributed to the Masing hardening. After yielding, obvious partitioning of tensile strain was detected in the gradient nano-grained structure, which indicates the existence of hetero-deformation induced (HDI) hardening effect and could account for the higher flow stress of the gradient nano-grained structure than that calculated by the rule of mixture from its homogenous nano-grained (NG) structured counterparts. Moreover, partitioning of stacking fault factor (corresponding to the partitioning of tensile strain), which demonstrates the intensity of dislocation behaviors, was also observed in the gradient nano-grained structure. The differences of factors for each grain size area were found to be smaller in the gradient nano-grained structure than those of its homogeneous nano-grained structured counterparts, which indicates the influence of forward stress and back stress on dislocation motion near the zone boundary between the hard zone with smaller grains and the soft zone with larger grains, further verifying the presence of hetero-deformation induced hardening in the gradient nano-grained structure.

KEYWORDS

molecular dynamics, gradient nano-grained, cryogenic temperature, hetero-deformation induced hardening, stacking fault factor

1 Introduction

The novel single-phase high- and medium-entropy alloys (HEA/MEA) (Cantor et al., 2004; Yeh et al., 2004; Gludovatz et al., 2016; Jo et al., 2017; Yang et al., 2018; Gan et al., 2019; George et al., 2019; Cui et al., 2022), containing three or more elements with equal molar fraction in general, have emerged recently and aroused great interest due to their excellent mechanical properties at ambient and cryogenic temperatures. Previous studies (Otto et al., 2013; Gludovatz et al., 2014; Schuh et al., 2015; Gludovatz et al., 2016; Miao et al., 2017; Yoshida et al., 2017; Zhang et al., 2017; Ma et al., 2018; Yang et al., 2018; Slone et al., 2019; Yang M. et al., 2019) have demonstrated that the random distribution of the atoms lowers the energy penalty for the formation of stacking fault (SF), rendering low stacking fault energy (SFE). The SFE of such alloys can even be negative at cryogenic temperature (Zhang et al., 2017), resulting in high propensity for twinning and phase transformation. The transition of the dominant deformation

mechanism from dislocation activities to deformation twins (DTs) then leads to better tensile and fracture properties than that at ambient temperature (Gludovatz et al., 2014; Gludovatz et al., 2016; Yang et al., 2018; Shi et al., 2019; Slone et al., 2019; Yang et al., 2020; Han et al., 2021; Ma et al., 2021). Moreover, recent work suggests that tailoring the local chemical order leads to non-uniform and locally tunable SFE in this sort of alloys (Ding et al., 2018), which may facilitate twinning and phase transformation at positions with lower fluctuated SFE.

Nano-grained (NG) metals and alloys usually have ultra-high strength, but show reduced ductility compared to their coarse grained (CG) counterparts. With increasing grain size, the ductility and strain hardening rate in most homogeneous structured metals are improved while the strength is sacrificed, an effect referred to as the strength–ductility trade-off (Koch et al., 1999; Valiev, 2004; Meyers et al., 2006; Ritchie, 2011; Wei et al., 2014). Materials with gradient nano-grained (GNG) structure, where the grain size increases from NG surface layers to CG core, have drawn widespread interest due to their excellent combination of strength and ductility (Wu X. et al., 2014; Wu X. L. et al., 2014; Wu et al., 2016; Li et al., 2017; Ma et al., 2019; Yang M.-X. et al., 2019; Yuan et al., 2019; Wu and Zhu, 2021). In the GNG structure, the mechanical incompatibility caused by gradient in grain size induces strain gradient, which leads to strong hetero-deformation induced (HDI) hardening and results in better mechanical properties (Yang et al., 2016; Wu and Zhu, 2021). In previous studies on CrCoNi MEA (Wen et al., 2020; Liu et al., 2021), this strategy has also been utilized to enhance the mechanical properties of the material.

Atomistic simulations have been proven to have advantages for investigating the microscopic deformation mechanisms of nanostructured metals, in which the real-time microstructural evolution of the system (snapshots), the atomistic and macroscopic stress and strain, and the stress state can be examined in detail (Yamakov et al., 2002; Schiøtz and Jacobsen, 2003; van Swygenhoven et al., 2004; Li et al., 2010). In previous studies (Widom et al., 2014; Li et al., 2016; Yuan et al., 2020; Ma et al., 2021), molecular dynamics (MD) simulations have been utilized to elucidate the atomistic deformation mechanisms in HEAs and MEAs. For instance, a hybrid Monte Carlo/MD method is applied to investigate the temperature-dependent chemical order in a HEA containing refractory metals Mo-Nb-Ta-W (Widom et al., 2014). The uniaxial tensile behaviors of the AlCrFeCuNi HEA are studied with MD simulation to analyze the evolution of defects (Li et al., 2016). For CrCoNi MEA, MD simulations have helped to study the nano-twinning behaviors (Yuan et al., 2020) and the effects of phase- and interface strengthening on the mechanical properties (Ma et al., 2021). Besides, MD simulations have also helped to investigate the deformation behaviors in hetero-structured materials (Li et al., 2015; Yuan et al., 2020). For example, in GNG structure of BCC Fe, MD method has demonstrated the stress state change and difference of deformation mechanisms in different-sized grains (Li et al., 2015). Using MD method, tensile strain partitioning is observed in CrCoNi MEA with heterogeneous grain structures under uniaxial tensile loadings (Yuan et al., 2020).

MD simulations may provide insights for the atomistic tensile deformation mechanisms either in HEA/MEA or in hetero-structured materials. In this regard, large-scale MD simulations were utilized in this work to investigate the tensile deformation behaviors of CrCoNi MEA with GNG structure and compare them with that of homogeneous NG structures with various grain sizes at cryogenic temperature.

2 Simulation techniques

The atomistic simulations were carried out utilizing the open source Large-scale Atomic/Molecular Massively Parallel Simulator (LAMMPS) (Plimpton, 1995) and the force reaction between atoms was simulated by an EAM potential developed by Farkas (Farkas and Caro, 2018).

2.1 Simulation model

In this study, five configurations are considered, i.e., the GNG structure with grain size increasing gradually from 12 to 96 nm, similar to the structure adopted in the work of (Li et al., 2015), and four homogeneous NG structures with grain size of 12, 24, 48 and 96 nm, respectively. The relaxed structures for the five configurations are demonstrated in Figure 1, where the atoms are colored based on the common neighbor analysis (CNA) values. The red color stands for dislocation core and grain boundary (GB) atoms, the blue color stands for HCP atoms and the perfect FCC atoms which are not shown in Figure 1. Aside from the red GB atoms, blue HCP atoms that mainly represent stacking faults could also be observed in Figure 1, which are believed to result from the energy minimization steps discussed later. With random orientation angles, the GNG structure contains 201 grains and the four homogeneous structures contain 1,440, 360, 96 and 24 grains, respectively. In order to investigate the deformation features of GNG structure, a columnar grain structure with [110]-textured simulation cells was utilized so that the grains larger than those possible in fully 3-dimensional simulations could be simulated, similar to the configurations adopted in previous researches (Yuan and Wu, 2013; Yuan et al., 2020). The GNG-structured samples and homogeneous NG-structured samples with grain size of 12 and 24 nm have dimensions (x × y × z) of 288 nm^3 × 623.54 nm^3 × 1.51 nm^3, with approximately 24,400,000 atoms. The homogeneous NG-structured samples with grain size of 48 and 96 nm have dimensions (x × y × z) of 288 nm^3 × 665.11 nm^3 × 1.51 nm^3, with approximately 26,000,000 atoms. All the simulation cells contain 12-layer atoms in z direction. Periodic boundary conditions were applied in all three directions during simulations.

2.2 Simulation process

The as-created samples were first subjected to energy minimization utilizing the conjugate gradient method before tensile deformation, and then gradually heated up to 77 K and finally relaxed under both 0 bar pressure in all three directions and the temperature 77 K for enough time (100 ps) to reach equilibrium using the Nose/Hoover isobaric-isothermal ensemble (NPT). Then, uniaxial tensile loading was imposed on the relaxed samples along x direction with a constant strain rate of 5×10^8 s^{-1} to a total tensile true strain of 15%. During the tensile loading, the overall pressures in the *y* and *z* directions were kept to be zero. In order to investigate the strain partitioning phenomenon between grains with different sizes, the atomic Green-Lagrangian strain tensor, which is based on atomic deformation gradient tensor derived from particle displacement vectors, was computed for each particle by OVITO (Stukowski, 2010) setting the cutoff radius to .5 nm. The relaxed structures before tensile loading were chosen to be the reference frame.

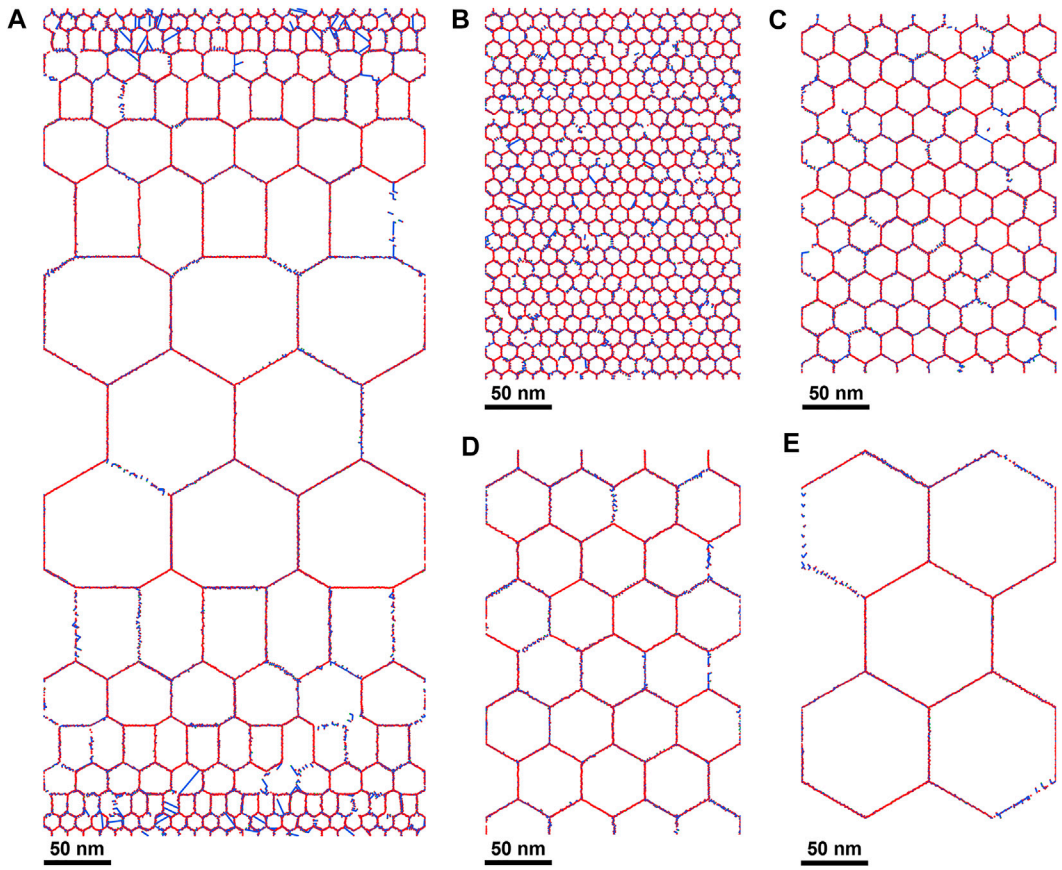

FIGURE 1
The relaxed tensile configuration of **(A)** GNG structured model and parts of homogeneous NG structured models with **(B)** 12 nm grains, **(C)** 24 nm grains, **(D)** 48 nm grains and **(E)** 96 nm grains.

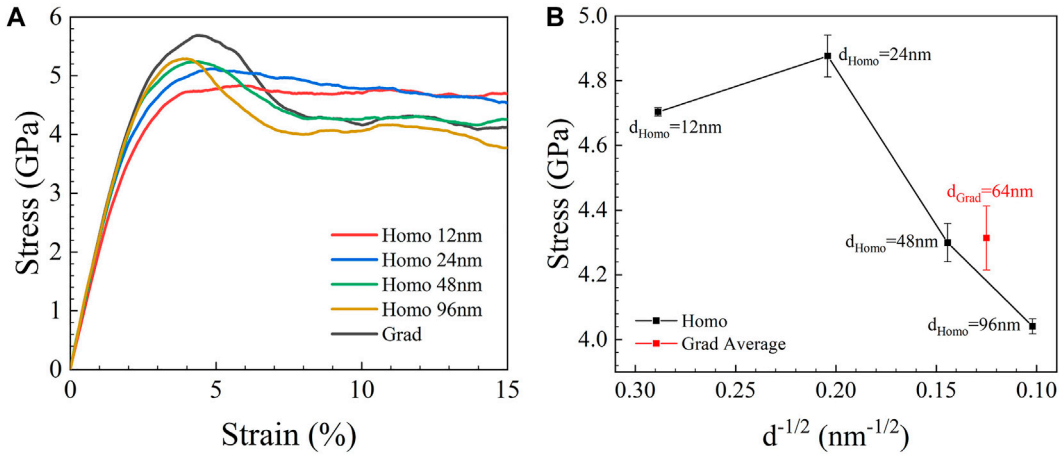

FIGURE 2
(A) Stress-Strain curves. **(B)** Flow stresses of the five configurations.

3 Results and discussions

The stress-strain curves for the five structures are juxtaposed in Figure 2A. At the elastic stage, the NG structure with 12 nm grains demonstrates a slightly lower Young's modulus, which could be attributed to the higher volume fraction of grain boundary and triple junction (Shen et al., 1995; Zhou et al., 2003). For the GNG structure and homogeneous NG structures with grain size larger than

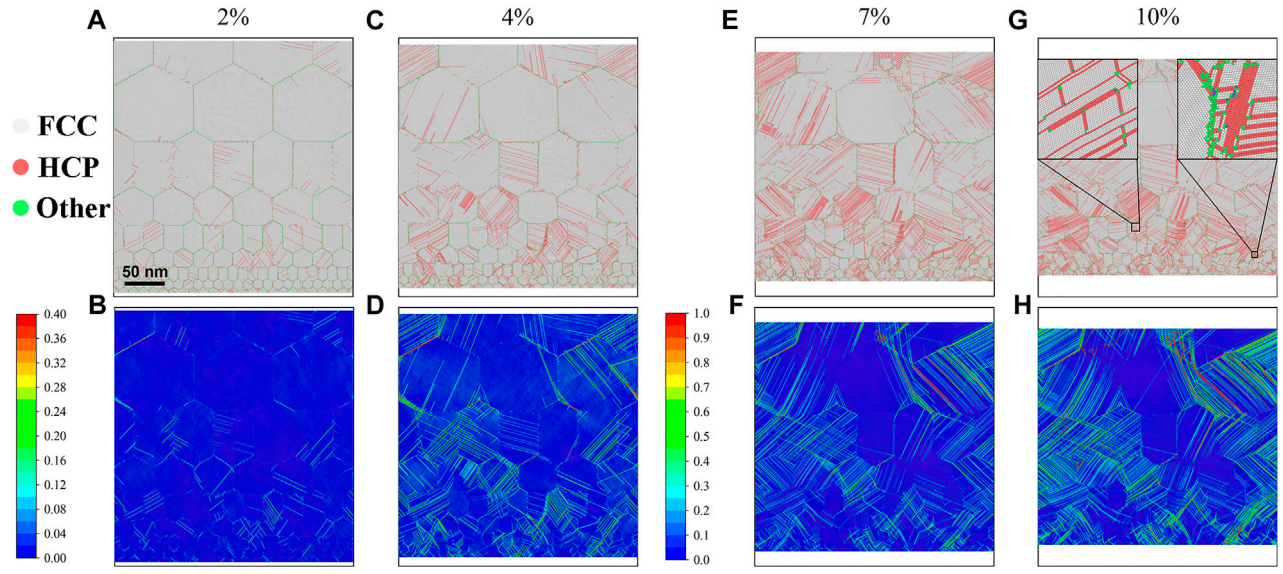

FIGURE 3
Snapshots from GNG structured model of atomistic structure and atomic tensile strain at applied tensile strain of **(A,B)** 2%, **(C,D)** 4%, **(E,F)** 7% and **(G,H)** 10%.

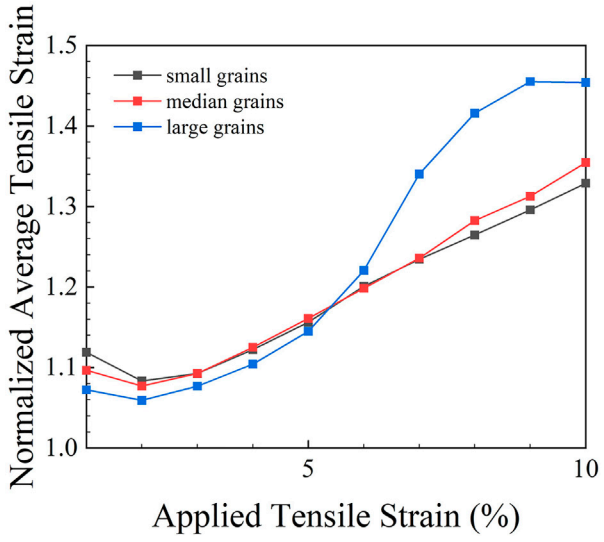

FIGURE 4
Partitioning of average tensile strain in x-axis in GNG structured model.

24 nm, tensile stress was observed to rise with strain to a certain peak stress after elastic stage, where strong strain hardening is showcased, before gradually decreasing to a steady-state value. The higher deformation rate employed in MD simulations, which deviates from the experimental scenarios (Yang et al., 2018; Slone et al., 2019), is considered to account for the stress overshoot phenomenon (Schiøtz and Jacobsen, 2003; Pan et al., 2008; Vo et al., 2009). The peak stress reaches a value over 5 GPa, which was in line with previous computational studies of NG HEA and MEA under cryogenic condition (Yuan et al., 2020; Zhang and Shibuta, 2020). Moreover, the GNG structure exhibits a higher yield stress than homogeneous NG structures. In Figure 2B, the flow stresses for the five structures are computed by the average tensile stress within applied tensile strain of 7%–10%. The average grain size of the GNG structured model is approximated to be 64 nm, calculated as the weighted average of the grain size over the volume occupied by grains of this size in the model. The flow stresses of the homogeneous NG structures agree with the Hall-Petch relation (Hansen, 2004) and the previous MD study on Nanocrystalline Copper (Schiøtz and Jacobsen, 2003), which reports a critical grain size (~15 nm) of FCC metal which leads to a maximum strength. The flow stress of the GNG structure, marked by the red dot, lies above the interpolated flow stress value of its homogenous NG structured counterpart, implying extra strengthening effects from the GNG structure, which will be discussed later.

In Figures 3A–D, snapshots from GNG structure at applied tensile strain of 2% and 4% of atomic tensile strain contours and on atomistic structures are demonstrated. Similar to previous study (Yuan et al., 2020), shortly after elastic deformation stage, most grains yield successively under the rising tensile load due to the variance in their size and orientation, which indicates an elasto-plastic transition. Therefore, Masing hardening (Skelton et al., 1997) should account for the strong strain hardening at this stage. Moreover, part of the reason for the higher yield stress of GNG structure could be manifest with the help of the snapshot. In the GNG structure, the defect density is higher in small grains during the elasto-plastic transition stage, approximately between 2% and 4% applied tensile strain, which implies that small grains carry more tensile strain at that stage. As a result, the elasticity of the large grains with generally higher Young's modulus are better preserved so that the hardening decay of them are partially impeded by the small grains at this stage, which helps maintain the high strain hardening rate before 4% applied tensile strain and contribute to the higher yield stress of the GNG structure. After the elasto-plastic transition stage, plastic deformation begins to take place in nearly all grains, so that the large grains start to

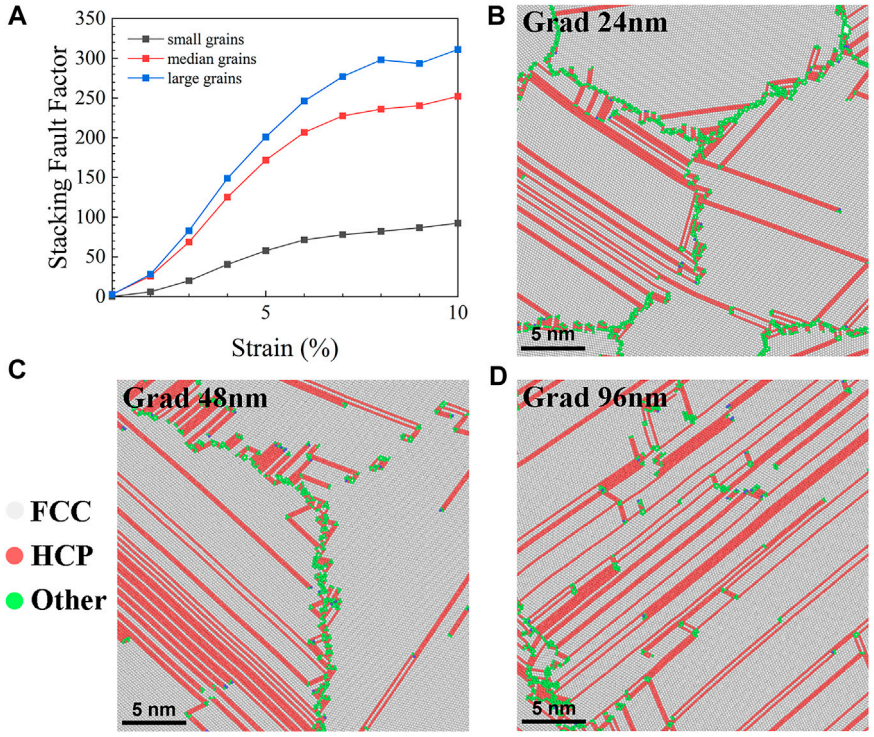

FIGURE 5
(A) Grain size dependency of stacking fault factor in GNG structured model. **(B–D)** Typical stacking fault pattern of 24, 48 and 96 nm grains in GNG structured model at applied tensile strain of 10%.

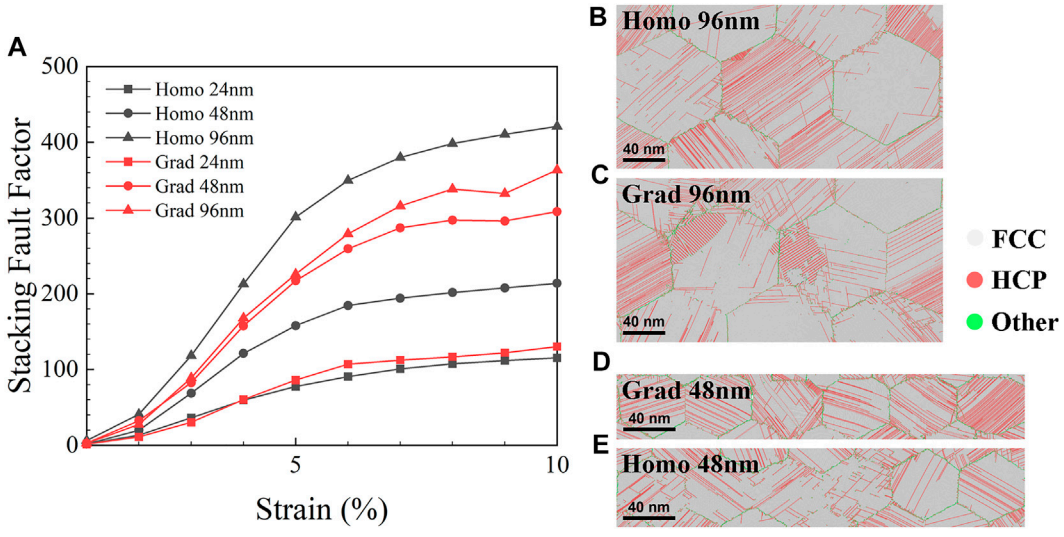

FIGURE 6
(A) Comparison of stacking fault factor from GNG structure and homogeneous NG structure in different sized grains. **(B–E)** Structure snapshot of 96 and 48 nm grains from homogeneous NG structured models and GNG structured model at applied tensile strain of 7%.

showcase less strength than the small grains according to Hall-Petch relation (Hansen, 2004), while the generally tougher small grains, on the contrary, begin to bolster the high stress value at applied tensile strain between 4% and 6%, as shown in Figure 2A.

The snapshots from GNG structure at applied tensile strain of 7% and 10% of atomic tensile strain contours and on atomistic structures are displayed in Figures 3E–H. Almost all grains are under plastic deformation with various defects. The low SFE of CrCoNi MEA at

cryogenic temperature engenders massive stacking faults that form networks and impede further propagation of defects (Xiao et al., 2021). Besides, as shown in Figure 3G, DTs and HCP transformation are observed, which are reported to improve the strength of the structure (Yuan et al., 2020). In the tensile strain contours, there are noticeably more red areas in large grains, which represent areas with large atomic tensile strain. In this case, a tensile strain partitioning is intuitively demonstrated in the strain contours, which can be further justified by the statistical data in Figure 4.

For the GNG structure, the normalized average tensile strain values demonstrated in Figure 4 are approximated for small grains, (12, 24 nm), median grains, (24, 48 nm), and large grains, (48, 96 nm), separately. The average value of Exx in Green-Lagrangian atomic strain tensor E, corresponding to the elongation in tensile direction, is computed over all atoms for each grain size area, then divided by the applied tensile strain for a clearer comparison. As shown in Figure 4, before the end of elasto-plastic transition stage, the large grains are reported to accommodate less tensile strain than medium and small grains, in line with the previous observation in Figures 3A–D of lower defect density in large grains, which verifies that Masing hardening occurs at this stage and further bolster the view that the elasticity of the large grains are better preserved at this stage so that they might have made critical contribution to the strong strain hardening when the applied tensile strain is smaller than 4%. With the applied tensile strain increasing above 5%, evident partitioning of tensile strain is showcased in the GNG structure. The large grains have accommodated the most tensile strain, while the small grains the least, which could be visually perceived in Figure 3H, corresponding to the previous studies on hetero-structured materials (Cong et al., 2009; Park et al., 2014; Wu et al., 2016; Yuan et al., 2020). The reason is that the small grains are generally harder than large grains during plastic deformation, according to Hall-Petch relation (Hansen, 2004). The observed strain partitioning would result in superior mechanical properties through the following process. As the neighboring zones accommodate different plastic strains due to strain partitioning, strain gradients will come to exist near the zone boundaries to maintain the continuity of plastic strain. To accommodate the strain gradient, geometrically necessary dislocations (GNDs) will be engendered near these interfaces, which will further generate long-range HDI stress near the zone boundaries that lead to higher global strength (Yang et al., 2016; Zhu and Wu, 2019; Wu and Zhu, 2021). Besides, the GNDs lead to higher dislocation density, so that the defects would have a better chance to entangle with each other, which also strengthen the structure (Li et al., 2015). These two mechanisms stemming from the strain partitioning are both believed to account for the higher flow stress of the GNG structure than its interpolated counterpart from homogenous NG structure, as shown in Figure 2B.

Beside strain partitioning, the partitioning of stacking fault factor is also observed in GNG structure and showcased in Figure 5A. The stacking fault factor is also calculated for three grain size area, namely small grains, (12, 24 nm), median grains, (24, 48 nm), and large grains, (48, 96 nm), separately. It is computed by the sum of HCP atoms in the corresponding grain size area, which characterizes the dislocation motion since mobile partial locations leave behind stacking faults, divided by the length of grain boundary, which represents the chance of dislocation formation, and then divided by the applied tensile strain for normalization. As a result, the factor shall reflect the intensity of dislocation motion during the tensile deformation process. As demonstrated in Figure 5A, the stacking fault factor for each grain sizes area in GNG structure generally rises with increasing applied tensile strain, indicating the proliferation of dislocations on the whole model. Besides, the stacking fault factor is reported to be the lowest in small grains and the highest in the large grains, which implies lowest intensity of dislocation motion in small grains and highest in large grains. This result correlates with the observation mentioned above that the large grains have accommodated the most tensile strain while the small grains the least during plastic deformation. Typical snapshots of structure for 24, 48 and 96 nm grains in the GNG structured model at applied tensile strain of 10% are displayed in Figures 5B–D.

In Figure 6A, the stacking fault factors of 24, 48 and 96 nm grains in GNG structure are compared with those in homogeneous NG structures. The factors of 24 and 48 nm grains in GNG structure are generally higher than those in homogeneous NG structure, while the 96 nm case is the opposite, which could be visualized in the snapshots of the relevant typical structure in Figures 6B–E. In other word, the values of stacking fault factor for GNG structure lie closer to each other than that for homogeneous NG counterpart, which further demonstrates the HDI hardening effect within the GNG structure. The reason for closer distribution of stacking fault factor in GNG structure could be attributed to the typical stress state near the zone boundary between the hard zone with smaller grains and soft zone with larger grains. In the soft zone, the GNDs generated by strain partitioning pile up against the zone boundary and induce manifest back stress, so that the resolved shear stress is reduced since the back stress is opposite to the applied shear stress. As a result, higher external stress could be accommodated in the soft zone, which makes the soft zone appear stronger and moderates the dislocation motion. On the other hand, in the hard zone, the forward stress induced by back stress acts in the direction of applied shear stress, which leads to a higher total stress, so that the hard zone appears weaker and more defects are generated. Eventually, the back stress and forward stress together produce the HDI stress that ameliorate the mechanical properties of the material (Wang et al., 2019; Zhu and Wu, 2019; Wu and Zhu, 2021).

4 Conclusion

In the present study, large-scale MD simulations have been utilized to study the tensile behaviors of a CrCoNi MEA with GNG structure, and the corresponding atomistic deformation mechanisms have also been revealed. The main findings can be summarized as follows.

1) Due to the Masing hardening, strong strain hardening was observed in the GNG structure at the elasto-plastic transition stage.
2) Obvious tensile strain partitioning was also observed in the GNG structure after yielding, indicating the existence of HDI hardening effect. The strain partitioning could also account for the higher flow stress of GNG structure than that calculated by the rule of mixture from its homogenous NG structured counterparts.
3) Similar to the tensile strain partitioning, partitioning of stacking fault factor (indicating the intensity of dislocation behaviors) was also observed in the GNG structure.
4) The differences of factors for each grain size area were found to be smaller in the GNG structure than those of its homogeneous NG structured counterparts. This observation could be attributed to the influence of forward stress and back stress on dislocation motion near the zone boundary between the hard zone with smaller grains and the soft zone with larger grains, further verifying the presence of HDI hardening in the GNG structure.

Therefore, the heterogeneous structure is found to have better tensile properties as compared to the corresponding homogeneous structure. The present findings should provide insights for optimizing heterogeneous microstructures to achieve superior mechanical properties in metals.

Data availability statement

The original contributions presented in the study are included in the article/Supplementary Material, further inquiries can be directed to the corresponding author.

Author contributions

YT, WC, and WW contributed to the conception and design of the study. YT and WC contributed to the simulation and wrote the first draft of the manuscript. WW contributed to manuscript revision.

Funding

This research was supported by the NSFC Basic Science Center Program for "Multiscale Problems in Non-linear Mechanics" (Grant No. 11988102) and the National Natural Science Foundation of China (Grant No. 52192591).

Acknowledgments

The authors would like to thank Fuping Yuan for his guidance and financial support.

Conflict of interest

The authors declare that the research was conducted in the absence of any commercial or financial relationships that could be construed as a potential conflict of interest.

Publisher's note

All claims expressed in this article are solely those of the authors and do not necessarily represent those of their affiliated organizations, or those of the publisher, the editors and the reviewers. Any product that may be evaluated in this article, or claim that may be made by its manufacturer, is not guaranteed or endorsed by the publisher.

References

Cantor, B., Chang, I., Knight, P., and Vincent, A. (2004). Microstructural development in equiatomic multicomponent alloys. *Mater. Sci. Eng. A* 375-377, 213–218. doi:10.1016/j.msea.2003.10.257

Cong, Z. H., Jia, N., Sun, X., Ren, Y., Almer, J., and Wang, Y. D. (2009). Stress and strain partitioning of ferrite and martensite during deformation. *Metallurgical Mater. Trans. A* 40 (6), 1383–1387. doi:10.1007/s11661-009-9824-2

Cui, K., Liaw, P. K., and Zhang, Y. (2022). Cryogenic-mechanical properties and applications of multiple-basis-element alloys. *Metals* 12 (12), 2075. doi:10.3390/met12122075

Ding, J., Yu, Q., Asta, M., and Ritchie, R. O. (2018). Tunable stacking fault energies by tailoring local chemical order in CrCoNi medium-entropy alloys. *Proc. Natl. Acad. Sci. U. S. A.* 115 (36), 8919–8924. doi:10.1073/pnas.1808660115

Farkas, D., and Caro, A. (2018). Model interatomic potentials and lattice strain in a high-entropy alloy. *J. Mater. Res.* 33 (19), 3218–3225. doi:10.1557/jmr.2018.245

Gan, B., Wheeler, J. M., Bi, Z., Liu, L., Zhang, J., and Fu, H. (2019). Superb cryogenic strength of equiatomic CrCoNi derived from gradient hierarchical microstructure. *J. Mater. Sci. Technol.* 35 (6), 957–961. doi:10.1016/j.jmst.2018.12.002

George, E. P., Raabe, D., and Ritchie, R. O. (2019). High-entropy alloys. *Nat. Rev. Mater.* 4 (8), 515–534. doi:10.1038/s41578-019-0121-4

Gludovatz, B., Hohenwarter, A., Catoor, D., Chang, E. H., George, E. P., and Ritchie, R. O. (2014). A fracture-resistant high-entropy alloy for cryogenic applications. *Sci. (New York, N.Y.)* 345 (6201), 1153–1158. doi:10.1126/science.1254581

Gludovatz, B., Hohenwarter, A., Thurston, K. V. S., Bei, H., Wu, Z., George, E. P., et al. (2016). Exceptional damage-tolerance of a medium-entropy alloy CrCoNi at cryogenic temperatures. *Nat. Commun.* 7 (1), 10602. doi:10.1038/ncomms10602

Han, Y., Li, H., Feng, H., Li, K., Tian, Y., and Jiang, Z. (2021). Simultaneous enhancement in strength and ductility of Fe50Mn30Co10Cr10 high-entropy alloy via nitrogen alloying. *J. Mater. Sci. Technol.* 65, 210–215. doi:10.1016/j.jmst.2020.04.072

Hansen, N. (2004). Hall–Petch relation and boundary strengthening. *Scr. Mater.* 51 (8), 801–806. doi:10.1016/j.scriptamat.2004.06.002

Jo, Y. H., Jung, S., Choi, W. M., Sohn, S. S., Kim, H. S., Lee, B. J., et al. (2017). Cryogenic strength improvement by utilizing room-temperature deformation twinning in a partially recrystallized VCrMnFeCoNi high-entropy alloy. *Nat. Commun.* 8, 15719. doi:10.1038/ncomms15719

Koch, C. C., Morris, D., Lu, K., and Inoue, A. (1999). Ductility of nanostructured materials. *MRS Bull.* 24 (2), 54–58. doi:10.1557/S0883769400051551

Li, J., Fang, Q., Liu, B., Liu, Y., and Liu, Y. (2016). Mechanical behaviors of AlCrFeCuNi high-entropy alloys under uniaxial tension via molecular dynamics simulation. *RSC Adv.* 6 (80), 76409–76419. doi:10.1039/C6RA16503F

Li, J., Weng, G., Chen, S., and Wu, X. (2017). On strain hardening mechanism in gradient nanostructures. *Int. J. Plasticity* 88, 89–107. doi:10.1016/j.ijplas.2016.10.003

Li, W., Yuan, F., and Wu, X. (2015). Atomistic tensile deformation mechanisms of Fe with gradient nano-grained structure. *AIP Adv.* 5 (8), 087120. doi:10.1063/1.4928448

Li, X., Wei, Y., Lu, L., Lu, K., and Gao, H. (2010). Dislocation nucleation governed softening and maximum strength in nano-twinned metals. *Nature* 464 (7290), 877–880. doi:10.1038/nature08929

Liu, Y., He, Y., and Cai, S. (2021). Effect of gradient microstructure on the strength and ductility of medium-entropy alloy processed by severe torsion deformation. *Mater. Sci. Eng. A* 801, 140429. doi:10.1016/j.msea.2020.140429

Ma, X., Li, F., Sun, Z., Hou, J., Fang, X., Zhu, Y., et al. (2019). Achieving gradient martensite structure and enhanced mechanical properties in a metastable β titanium alloy. *Metallurgical Mater. Trans. A* 50 (5), 2126–2138. doi:10.1007/s11661-019-05157-5

Ma, Y., Yang, M., Yuan, F., and Wu, X. (2021). Deformation induced hcp nano-lamella and its size effect on the strengthening in a CoCrNi medium-entropy alloy. *J. Mater. Sci. Technol.* 82, 122–134. doi:10.1016/j.jmst.2020.12.017

Ma, Y., Yuan, F., Yang, M., Jiang, P., Ma, E., and Wu, X. (2018). Dynamic shear deformation of a CrCoNi medium-entropy alloy with heterogeneous grain structures. *Acta Mater.* 148, 407–418. doi:10.1016/j.actamat.2018.02.016

Meyers, M. A., Mishra, A., and Benson, D. J. (2006). Mechanical properties of nanocrystalline materials. *Prog. Mater. Sci.* 51 (4), 427–556. doi:10.1016/j.pmatsci.2005.08.003

Miao, J., Slone, C., Smith, T., Niu, C., Bei, H., Ghazisaeidi, M., et al. (2017). The evolution of the deformation substructure in a Ni-Co-Cr equiatomic solid solution alloy. *Acta Mater.* 132, 35–48. doi:10.1016/j.actamat.2017.04.033

Otto, F., Dlouhy, A., Somsen, C., Bei, H., Eggeler, G., and George, E. (2013). The influences of temperature and microstructure on the tensile properties of a CoCrFeMnNi high-entropy alloy. *Acta Mater.* 61 (15), 5743–5755. doi:10.1016/j.actamat.2013.06.018

Pan, Z., Li, Y., and Wei, Q. (2008). Tensile properties of nanocrystalline tantalum from molecular dynamics simulations. *Acta Mater.* 56 (14), 3470–3480. doi:10.1016/j.actamat.2008.03.025

Park, K., Nishiyama, M., Nakada, N., Tsuchiyama, T., and Takaki, S. (2014). Effect of the martensite distribution on the strain hardening and ductile fracture behaviors in dual-phase steel. *Mater. Sci. Eng. A* 604, 135–141. doi:10.1016/j.msea.2014.02.058

Plimpton, S. (1995). Fast Parallel algorithms for short-range molecular dynamics. *J. Comput. Phys.* 117 (1), 1–19. doi:10.1006/jcph.1995.1039

Ritchie, R. O. (2011). The conflicts between strength and toughness. *Nat. Mater.* 10 (11), 817–822. doi:10.1038/nmat3115

Schiøtz, J., and Jacobsen, K. W. (2003). A maximum in the strength of nanocrystalline copper. *Sci. (New York, N.Y.)* 301 (5638), 1357–1359. doi:10.1126/science.1086636

Schuh, B., Mendez-Martin, F., Volker, B., George, E., Clemens, H., Pippan, R., et al. (2015). Mechanical properties, microstructure and thermal stability of a nanocrystalline CoCrFeMnNi high-entropy alloy after severe plastic deformation. *Acta Mater.* 96, 258–268. doi:10.1016/j.actamat.2015.06.025

Shen, T. D., Koch, C., Tsui, T., and Pharr, G. (1995). On the elastic moduli of nanocrystalline Fe, Cu, Ni, and Cu–Ni alloys prepared by mechanical milling/alloying. *J. Mater. Res.* 10 (11), 2892–2896. doi:10.1557/JMR.1995.2892

Shi, P., Ren, W., Zheng, T., Ren, Z., Hou, X., Peng, J., et al. (2019). Enhanced strength-ductility synergy in ultrafine-grained eutectic high-entropy alloys by inheriting microstructural lamellae. *Nat. Commun.* 10 (1), 489. doi:10.1038/s41467-019-08460-2

Skelton, R. P., Maier, H. J., and Christ, H.-J. (1997). The Bauschinger effect, Masing model and the Ramberg–Osgood relation for cyclic deformation in metals. *Mater. Sci. Eng. A* 238 (2), 377–390. doi:10.1016/S0921-5093(97)00465-6

Slone, C. E., Miao, J., George, E., and Mills, M. (2019). Achieving ultra-high strength and ductility in equiatomic CrCoNi with partially recrystallized microstructures. *Acta Mater.* 165, 496–507. doi:10.1016/j.actamat.2018.12.015

Stukowski, A. (2010). Visualization and analysis of atomistic simulation data with OVITO–the Open Visualization Tool. *Model. Simul. Mater. Sci. Eng.* 18 (1), 015012. doi:10.1088/0965-0393/18/1/015012

Valiev, R. (2004). Nanostructuring of metals by severe plastic deformation for advanced properties. *Nat. Mater.* 3 (8), 511–516. doi:10.1038/nmat1180

van Swygenhoven, H., Derlet, P. M., and Frøseth, A. G. (2004). Stacking fault energies and slip in nanocrystalline metals. *Nat. Mater.* 3 (6), 399–403. doi:10.1038/nmat1136

Vo, N. Q., Averback, R. S., Bellon, P., and Caro, A. (2009). Yield strength in nanocrystalline Cu during high strain rate deformation. *Scr. Mater.* 61 (1), 76–79. doi:10.1016/j.scriptamat.2009.03.003

Wang, Y. F., Huang, C., He, Q., Guo, F., Wang, M., Song, L., et al. (2019), Heterostructure induced dispersive shear bands in heterostructured Cu. *Scr. Mater.* 170, 76–80. doi:10.1016/j.scriptamat.2019.05.036

Wei, Y., Li, Y., Zhu, L., Liu, Y., Lei, X., Wang, G., et al. (2014). Evading the strength-ductility trade-off dilemma in steel through gradient hierarchical nanotwins. *Nat. Commun.* 5, 3580. doi:10.1038/ncomms4580

Wen, R., You, C., Zeng, L., Wang, H., and Zhang, X. (2020). Achieving a unique combination of strength and ductility in CrCoNi medium-entropy alloy via heterogeneous gradient structure. *J. Mater. Sci.* 55 (26), 12544–12553. doi:10.1007/s10853-020-04870-6

Widom, M., Huhn, W. P., Maiti, S., and Steurer, W. (2014). Hybrid Monte Carlo/molecular dynamics simulation of a refractory metal high entropy alloy. *Metallurgical Mater. Trans. A* 45 (1), 196–200. doi:10.1007/s11661-013-2000-8

Wu, X., Jiang, P., Chen, L., Yuan, F., and Zhu, Y. T. (2014). Extraordinary strain hardening by gradient structure. *Proc. Natl. Acad. Sci. U. S. A.* 111 (20), 7197–7201. doi:10.1073/pnas.1324069111

Wu, X. L., Jiang, P., Chen, L., Zhang, J. F., Yuan, F. P., and Zhu, Y. T. (2014). Synergetic strengthening by gradient structure. *Mater. Res. Lett.* 2 (4), 185–191. doi:10.1080/21663831.2014.935821

Wu, X. L., Yang, M., Yuan, F., Chen, L., and Zhu, Y. (2016). Combining gradient structure and TRIP effect to produce austenite stainless steel with high strength and ductility. *Acta Mater.* 112, 337–346. doi:10.1016/j.actamat.2016.04.045

Wu, X., and Zhu, Y. T. (2021). in *Heterostructured materials: Novel materials with unprecedented mechanical properties/*. Editors Xiaolei Wu and Yuntian Zhu (Singapore: Jenny Stanford Publishing).

Xiao, J., Wu, N., Ojo, O., and Deng, C. (2021). Stacking fault and transformation-induced plasticity in nanocrystalline high-entropy alloys. *J. Mater. Res.* 36 (13), 2705–2714. doi:10.1557/s43578-021-00140-6

Yamakov, V., Wolf, D., Phillpot, S. R., Mukherjee, A. K., and Gleiter, H. (2002). Dislocation processes in the deformation of nanocrystalline aluminium by molecular-dynamics simulation. *Nat. Mater.* 1 (1), 45–49. doi:10.1038/nmat700

Yang, M-X., Zhou, L., Wang, C., Jiang, P., Yuan, F., Ma, E., et al. (2019). High impact toughness of CrCoNi medium-entropy alloy at liquid-helium temperature. *Scr. Mater.* 172, 66–71. doi:10.1016/j.scriptamat.2019.07.010

Yang, M., Li, R. G., Jiang, P., Yuan, F. P., Wang, Y. D., Zhu, Y. T., et al. (2019). Residual stress provides significant strengthening and ductility in gradient structured materials. *Mater. Res. Lett.* 7 (11), 433–438. doi:10.1080/21663831.2019.1635537

Yang, M., Pan, Y., Yuan, F., Zhu, Y., and Wu, X. (2016). Back stress strengthening and strain hardening in gradient structure. *Mater. Res. Lett.* 4 (3), 145–151. doi:10.1080/21663831.2016.1153004

Yang, M., Yan, D., Yuan, F., Jiang, P., Ma, E., and Wu, X. (2018). Dynamically reinforced heterogeneous grain structure prolongs ductility in a medium-entropy alloy with gigapascal yield strength. *Proc. Natl. Acad. Sci. U. S. A.* 115 (28), 7224–7229. doi:10.1073/pnas.1807817115

Yang, Z., Yang, M., Ma, Y., Zhou, L., Cheng, W., Yuan, F., et al. (2020). Strain rate dependent shear localization and deformation mechanisms in the CrMnFeCoNi high-entropy alloy with various microstructures. *Mater. Sci. Eng. A* 793, 139854. doi:10.1016/j.msea.2020.139854

Yeh, J.-W., Chen, S. K., Lin, S. J., Gan, J. Y., Chin, T. S., Shun, T. T., et al. (2004). Nanostructured high-entropy alloys with Multiple principal elements: Novel alloy design concepts and outcomes. *Adv. Eng. Mater.* 6 (5), 299–303. doi:10.1002/adem.200300567

Yoshida, S., Bhattacharjee, T., Bai, Y., and Tsuji, N. (2017). Friction stress and Hall-Petch relationship in CoCrNi equi-atomic medium entropy alloy processed by severe plastic deformation and subsequent annealing. *Scr. Mater.* 134, 33–36. doi:10.1016/j.scriptamat.2017.02.042

Yuan, F., Cheng, W., Zhang, S., Liu, X., and Wu, X. (2020). Atomistic simulations of tensile deformation in a CrCoNi medium-entropy alloy with heterogeneous grain structures. *Materialia* 9, 100565. doi:10.1016/j.mtla.2019.100565

Yuan, F., and Wu, X. (2013). Size effects of primary/secondary twins on the atomistic deformation mechanisms in hierarchically nanotwinned metals. *J. Appl. Phys.* 113 (20), 203516. doi:10.1063/1.4808096

Yuan, F., Yan, D., Sun, J., Zhou, L., Zhu, Y., and Wu, X. (2019). Ductility by shear band delocalization in the nano-layer of gradient structure. *Mater. Res. Lett.* 7 (1), 12–17. doi:10.1080/21663831.2018.1546238

Zhang, L., and Shibuta, Y. (2020). Inverse Hall-Petch relationship of high-entropy alloy by atomistic simulation. *Mater. Lett.* 274, 128024. doi:10.1016/j.matlet.2020.128024

Zhang, Z., Sheng, H., Wang, Z., Gludovatz, B., George, E. P., et al. (2017). Dislocation mechanisms and 3D twin architectures generate exceptional strength-ductility-toughness combination in CrCoNi medium-entropy alloy. *Nat. Commun.* 8, 14390. doi:10.1038/ncomms14390

Zhou, Y., Erb, U., Aust, K., and Palumbo, G. (2003). The effects of triple junctions and grain boundaries on hardness and Young's modulus in nanostructured Ni–P. *Scr. Mater.* 48 (6), 825–830. doi:10.1016/S1359-6462(02)00511-0

Zhu, Y., and Wu, X. (2019). Perspective on hetero-deformation induced (HDI) hardening and back stress. *Mater. Res. Lett.* 7 (10), 393–398. doi:10.1080/21663831.2019.1616331